Supplementary Information

Assessing the improved performance of freestanding, flexible graphene and carbon nanotube hybrid foams for lithium ion battery anodes

*Adam P. Cohn[1], Landon Oakes[1,2], Rachel Carter[1], Shahana Chatterjee[1], Andrew Westover[1,2], Keith Share[1,2], and Cary L. Pint[1,2,]**

[1] Department of Mechanical Engineering, Vanderbilt University, Nashville, TN 37235

[2] Interdisciplinary Materials Science Program, Vanderbilt University, Nashville, TN 37235

*Corresponding author: cary.l.pint@vanderbilt.edu

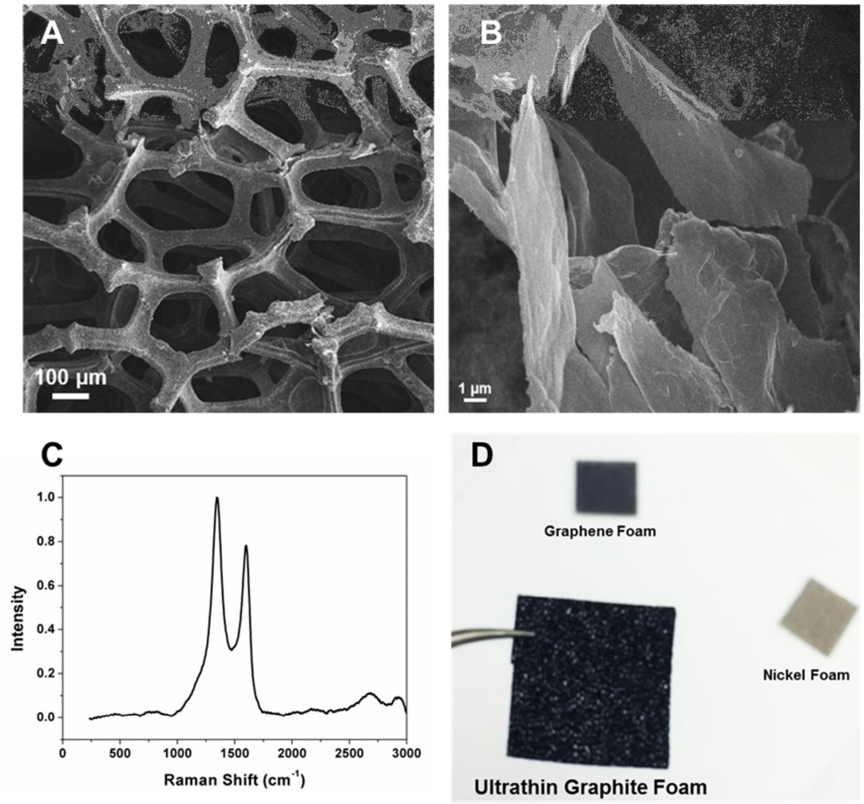

Fig. S1. (A) SEM image of the ultrathin graphite foam after etching in HCl. (B) SEM image of the ultrathin graphite showing graphite flakes. (C) Raman spectroscopic characterization (532 nm) of ultrathin graphite foam. (D) The ultrathin graphite foam after CVD.

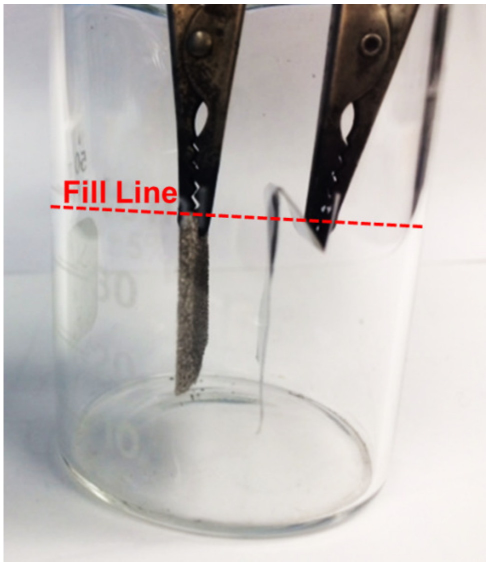

Fig. S2. EPD setup with the graphene/nickel foam electrode shown on the left and the counter electrode shown on the right.

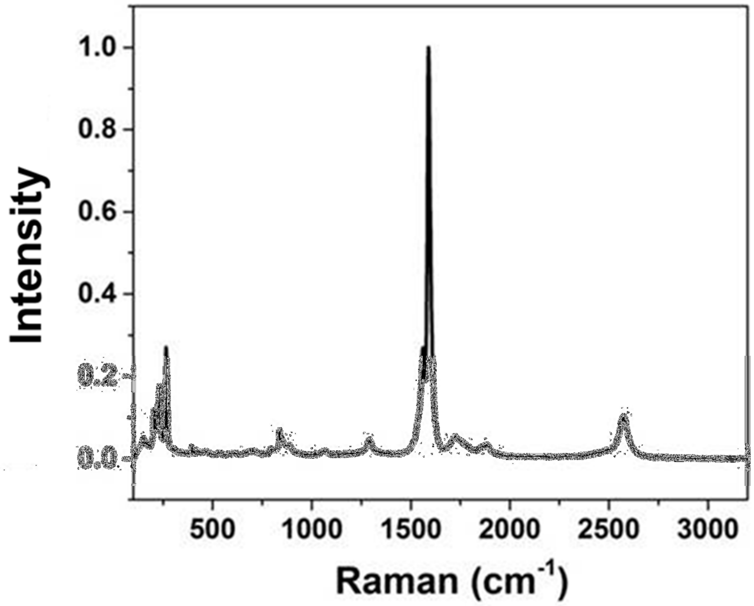

Fig. S3. Raman spectroscopic characterization (785 nm) of free-standing SWNT foam.

Additional Testing

Cyclic voltammetry performed on the hybrid graphene-SWNT device at different scan rates shows the time dependence of the reactions. At a fast CV scan rate of 50 mV/s, there is almost no low-voltage bulk storage based on the lack of a discernable shoulder in the positive CV scan (Fig. S4C). As the scan rate decreases, we see an increase in the proportion of low-voltage bulk storage and the emergence of a small, sharp peak. We also observe narrowing and shifting of the 1-2 V reaction peak.

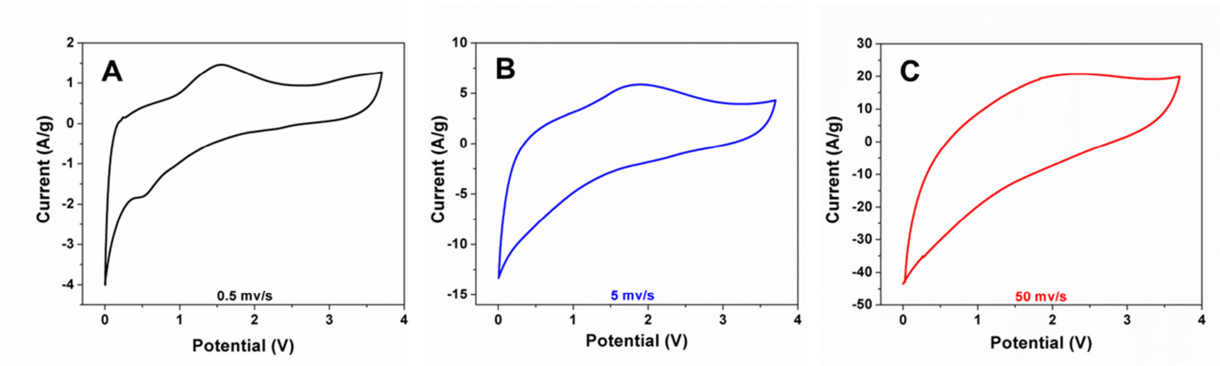

Fig. S4. Cyclic voltammetry profiles of the hybrid graphene-SWNT foam performed at (A) 0.5 mV/s, (B) 5 mV/s and (C) 50 mV/s.

Whereas we consistently observe the greatest capacity from the first discharge, the reversible capacity of our materials exhibit an increasing capacity over cycling that is especially apparent at slow rates. Shown in Fig. S5 is the first discharge, the second discharge and then the 300th discharge at 3.7 A/g for a hybrid graphene-SWNT device. As is evident from Fig. 5, the discharge capacity at the 300th cycle is situated between the first and second discharges. Whereas the origin of this effect requires further analysis, we anticipate the SEI layer formation on sp^2 carbon to be associated with the first charge, and further cycling the devices conditions the SEI layer to optimize surface storage characteristics on the graphene. This emphasizes the need to better understand the impact of surface characteristics on surface Faradaic reactions.

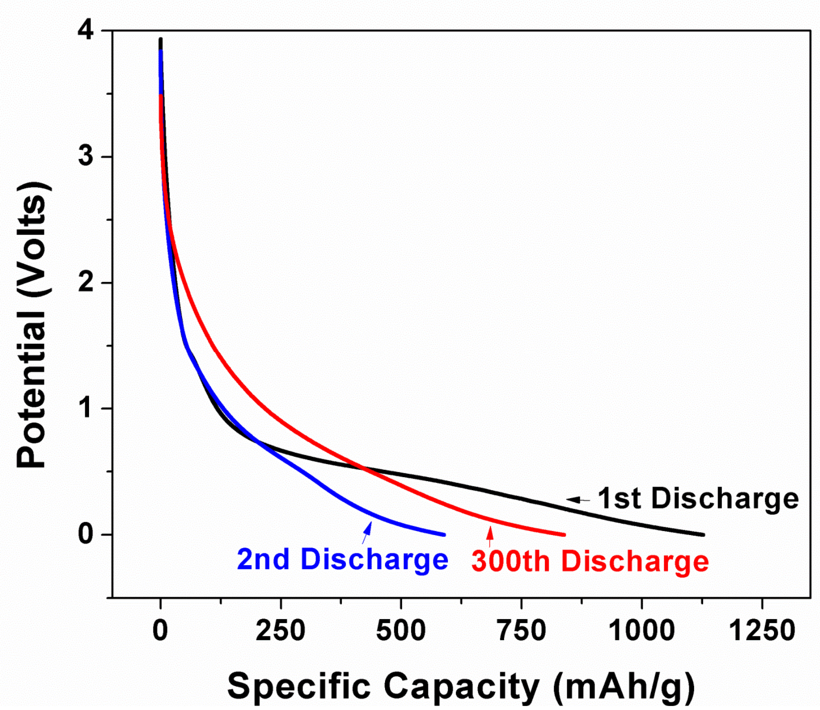

Fig. S5. Discharge profiles of the hybrid graphene-SWNT foam at 3.7 A/g before and after cycling.

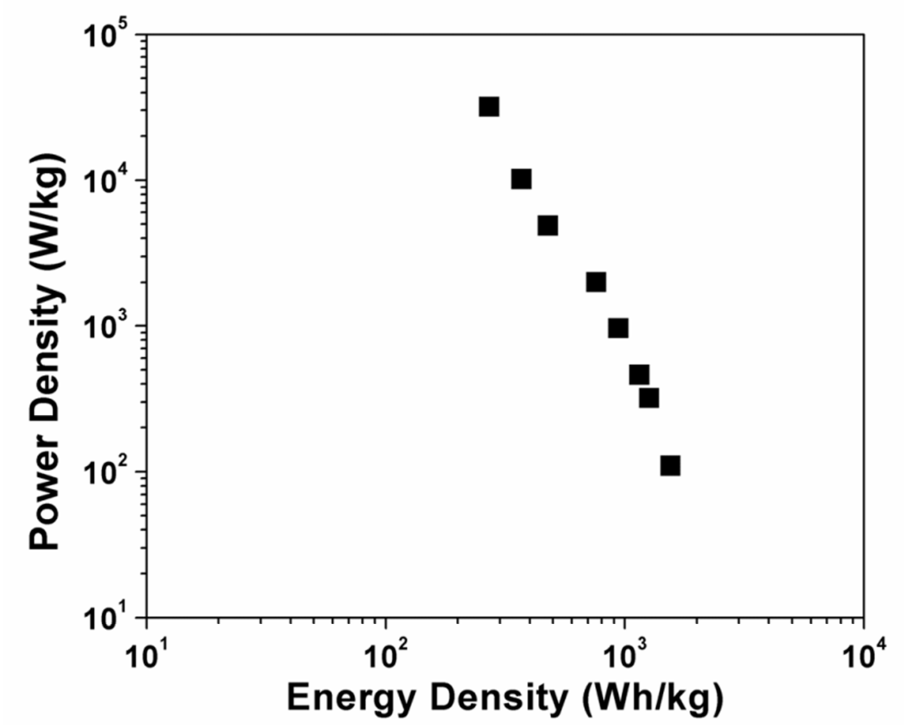

Fig. S6. Ragone analysis of the rate-dependent Galvanostatic characteristics with respect to a single graphene-SWNT hybrid electrode in a half-cell configuration.

In order to assess the energy-power characteristics of the graphene-SWNT hybrid devices, we performed Ragone analysis, which involves the numerical solution to:

$$E = \int_t I \times V(t) dt$$

Where the area under the *V(t)* curve from the Galvanostatic charging profile dictates the total amount of energy stored in the device. To then obtain Ragone plots, we calculate the power based upon the total energy stored over the discharge time, or $P = E/\Delta t$. This method yields the exact energy and power stored in the device with no approximations to the curve profile such as the typical use of $E = 0.5CV^2$ that is commonly applied in supercapacitors and can be extracted from the above equation assuming *V(t)* is a linear function.

Interlayer spacing of graphene

Using high-resolution transmission electron microscopy (HR-TEM) we examined multilayered graphene samples both with and without SWNT after EPD. TEM images, interlayer spacing maps, and FFT images are shown in Fig. S7. This interlayer (d-) spacing was measured in both materials to be 0.34 nm from both profile maps and FFTs. It should be noted that outside of the graphene fringes in both materials reside either SWNT/graphene (top) or graphene (bottom) that are out of the plane of focus. This result confirms that the presence of the SWNT do not change the properties of the graphene, and that the comparison between graphene-SWNT and graphene materials represents a controlled comparison between similar materials only differing by the presence of SWNTs on the surface in the first case.

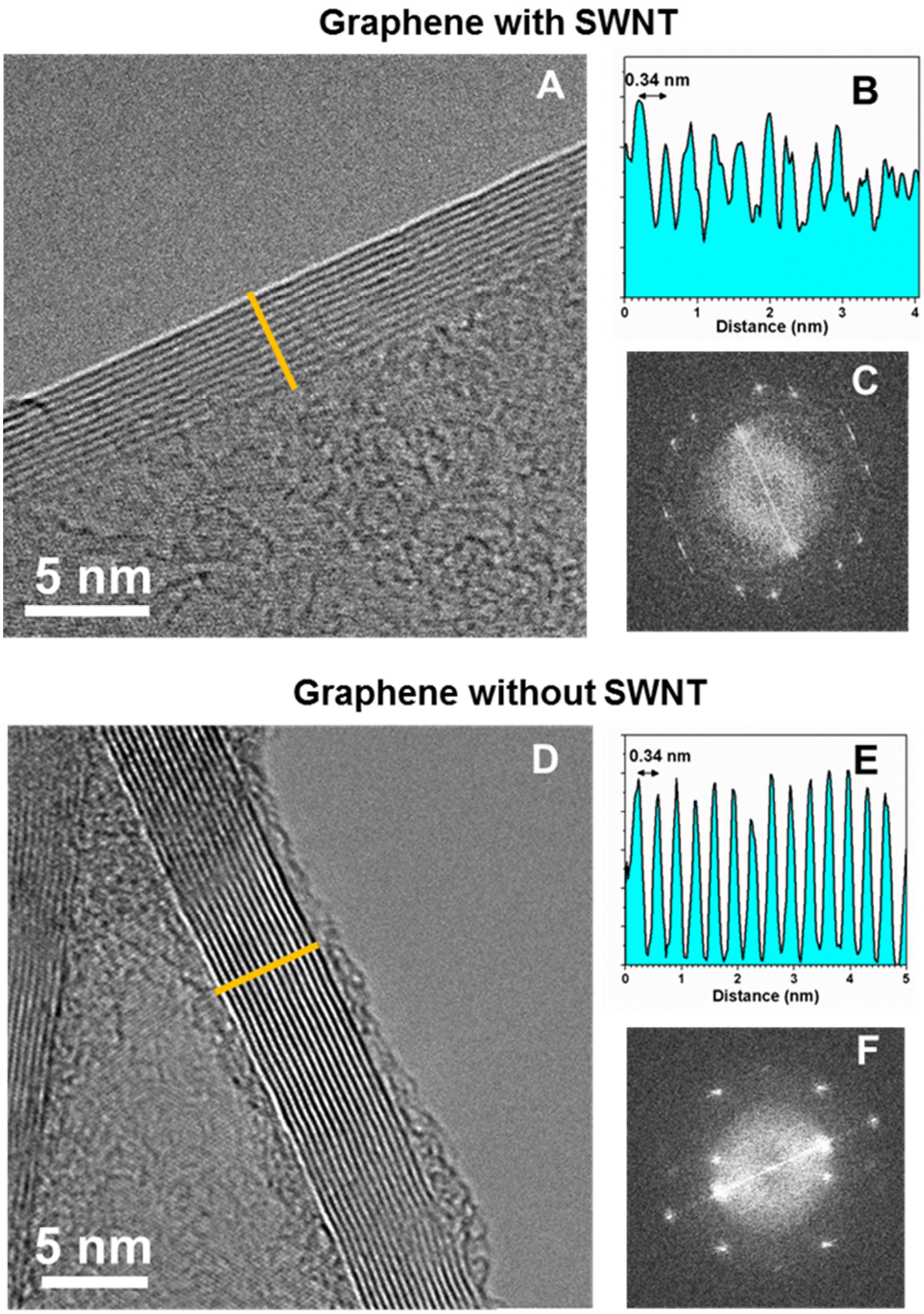

Fig. S7. Investigating d-spacing in multilayered graphene with and without SWNT. (a) cross-sectional TEM image of multilayered graphene with SWNT, (b) profile analysis showing spacing of ~0.34 nm and (c) FFT confirming spacing pattern ~0.34 nm. (d) cross-sectional TEM image of multilayered graphene without SWNT, (e) profile analysis showing spacing of ~0.34 nm and (f) FFT confirming spacing pattern ~0.34 nm.